An MRI-Derived Neuroanatomical Atlas of the Fischer 344 Rat Brain for Automated Anatomical Segmentation

*Dana Goerzen[a], Caitlin Fowler[b], Gabriel A. Devenyi[c,d], Jurgen Germann[c], Dan Madularu[c,d,e], M. Mallar Chakravarty[b,c,d], and Jamie Near[b,c,d]

a. Department of Neuroscience, McGill University, H3A 0G4, Montreal, Canada.

b. Department of Biological and Biomedical Engineering, McGill University, H3A 0G4, Montreal, Canada.

c. Centre d'Imagerie Cérébrale, Douglas Mental Health University Institute, H4H 1R3, Verdun, Canada.

d. Department of Psychiatry, McGill University, H3A 0G4, Montreal, Canada.

e. Centre for Translational Neuroimaging, Northeastern University, 02115, Boston, MA, USA

Corresponding Author:

Dana Goerzen

Email: dana.goerzen@mail.mcgill.ca

Telephone: (613)-449-0967

Acknowledgements:

This research was supported by the Canadian Institutes of Health Research (PJT - 148751) and the Fonds de la recherche en santé du Québec (Chercheurs Boursiers # 35275). GAD is supported in part by funding provided by Brain Canada, in partnership with Health Canada, for the Canadian Open Neuroscience Platform initiative.

Compliance with Ethical Standards

Competing Interests: The authors declare that they have no competing interests.

Funding: This research was supported by the Canadian Institutes of Health Research (PJT - 148751) and the Fonds de la recherche en santé du Québec (Chercheurs Boursiers # 35275). GAD is supported in part by funding provided by Brain Canada, in partnership with Health Canada, for the Canadian Open Neuroscience Platform initiative.

Ethical approval: All applicable international, national, and/or institutional guidelines for the care and use of animals were followed. All animal procedures and experiments were approved by the McGill University Animal Care Committee (UACC).

Author Contributions Statement: D.G generated and manually segmented the template image. D.G, C.F, and J.N wrote the main manuscript text. C.F, D.M, and J.N collected data. J.G, M.C and GAD provided statistical analyses. All authors reviewed the manuscript.

Data Availability Statement: The final anatomical segmentation volume along with the template brain, corresponding label descriptions, and a brain masking volume were each converted from MINC format into NIfTI format using the minc-toolkit `mnc2nii` function. All of the above are available for download and free use through the Near Lab website at https://www.nearlab.xyz/fischer344atlas in both NIfTI and the MINC 2.0 format – compatible with all MINC tools, as well as Pydpiper and RMINC software

Abstract:

This paper reports the development of a high-resolution 3-D MRI atlas of the Fischer 344 adult rat brain. The atlas is a 60 µm isotropic image volume composed of 256 coronal slices with 98 manually delineated structures and substructures. The atlas was developed using Pydpiper image registration pipeline to create an average brain image of 41 four-month-old male and female Fischer 344 rats. Slices in the average brain image were then digitally segmented, individually and bilaterally, on the basis of image contrast in conjunction with Paxinos and Watson's (2007) stereotaxic rat brain atlas. Summary statistics (mean and standard deviation of regional volumes) are reported for each brain region across the sample used to generate the atlas, and a statistical comparison of a chosen subset of regional brain volumes between male and female rats is presented. On average, the coefficient of variation of regional brain volumes across all rats in our sample was 5%, with no individual brain region having a coefficient of variation greater than 14%. A full description of methods used, as well as the atlas, the template that the atlas was derived from, and a masking file, can be found at https://www.nearlab.xyz/fischer344atlas. To our knowledge, this is the first MRI atlas created using Fischer 344 rats and will thus provide an appropriate neuroanatomical model for researchers working with this strain.

Graphical Abstract

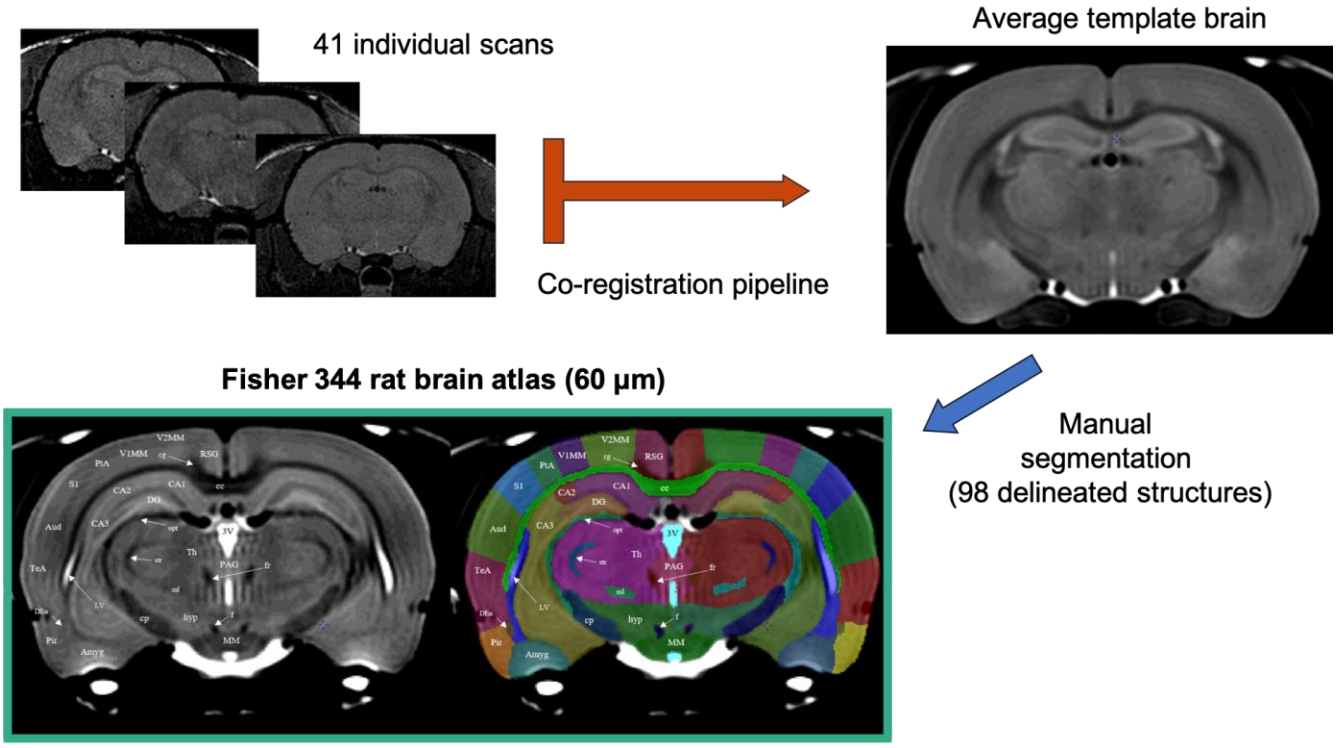

HIGHLIGHTS

- **Open-access high-resolution anatomical MRI template for Fischer 344 rat brain.**
- **Segmented atlas of 98 regions for use as a tool in Fischer 344 preclinical research paradigms.**
- **Analysis of population variability of regional brain volumes.**
- **Analysis of sex-differences in regional brain volumes**

KEYWORDS: Fischer 344; Structural MRI; Segmentation; Rat brain template; Digital brain atlas; Sex-differences;

1. INTRODUCTION:

In neuroscientific research involving preclinical rodent models, the ability to precisely identify and delineate anatomical brain regions is often a requirement (Nowinski, 2016). In the past, this identification was done using paper atlases such as Paxinos and Watson's (P&W) *The Rat Brain in Stereotaxic Coordinates* (Paxinos and Watson, 2007). However, with the increased prevalence of preclinical high-resolution magnetic resonance (MR) imaging in the past decade, digital neuroanatomical atlases have emerged in neuroinformatics research as a tool for quick and accurate identification of anatomical regions in laboratory animals (Lancelot et al, 2014). Digital atlases based on isotropic MRI provide flexibility over paper atlases by easily allowing interactive viewing of anatomical regions from arbitrary planes without distortion. This permits researchers to automatically record morphological information, such as the volume of brain regions, at an individual structural level (Chen et al, 2006; Dorr et al, 2008).

A number of digital rat brain atlases for different rat strains have previously been published and disseminated, as shown in **Table 1**. (Valdés-Hernández PA et al, 2011; Calabrese et al, 2013; Papp et al, 2014). The current study is motivated by the fact that there is currently no digital atlas for the Fischer 344 rat strain published in the literature or available online. Given that the Fischer 344 rat strain is commonly used in preclinical neuroscientific research (Perkin et al, 2018; Balogová et al, 2018; Fole et al, 2017), and given the emergence of novel transgenic rat models generated on a Fischer 344 background (TgF344-AD, Cohen et al 2013; APP21 & APP31, Agca et al 2008, PMID 18302776; F344 gpt delta, Hori et al 2019; PMID 30595204, etc.), a digital anatomical atlas of the Fischer 344 rat brain would be of value to the scientific community.

STUDY	Papp et al. (2014)	Calabrese et al. (2013)	Schwarz et al. (2006)	Rumple et al. (2013)	Johnson et al. (2012)	Valdes-Hernandez et al. (2011)	Current Study
RAT STRAIN	Sprague Dawley	Wistar	Sprague Dawley	Sprague Dawley	Wistar	Wistar	Fischer 344
RESOLUTION OF T2-WEIGHTED MRI	39 um^3	25 um^3	190 um^3	70 um^3 for P5 and P14, 125 um^3 for P72	25 um^3		60 um^3
MODALITY	MR and DTI	MR and DTI	MR only	MR and DTI	MR, DTI, and histology	MR only	MR only
SAMPLE SIZE (n)	1 male	5 males per timepoint	97 males	1 male and 1 female for P5 and P14, 5 females for P72	5 males	5 males per timepoint	41 mixed sex (24 male, 17 female)
AVERAGE MR USED	No	Yes	Yes	Yes	Yes	Yes	Yes
ATLAS REGIONS	Whole Brain	Whole Brain	Whole Brain	Whole Brain	Whole Brain	Whole Brain	Whole Brain
	Ex-vivo	Ex-vivo	In-vivo	In-vivo	Ex-vivo	In-vivo	In-vivo
LABEL METHOD	Semi-automatic (SNAP) and manual segmentation on MR.	MR average brains were aligned to conventional histological atlases.	Co-registration of average MR template to digital Paxinos and Watson atlas	Manual delineation in an iterative fashion based on T2 tissue contrast. Primarily delineated in coronal view, with sagittal and axial views used to verify segmentation.	Co-registration of average MR template to digital Paxinos and Watson histological atlas	Co-registration of average MR template to digital Paxinos and Watson histological atlas	Stepwise manual segmentation based on T2 contrast on MR template, in conjunction with Paxinos and Watson atlas.
NUMBER OF SEGMENTED STRUCTURES	118	26	468 from co-registered Paxinos and Watson histological atlas	P5: 39 structures P14: 45 structures P72: 29 structures	20	96	98
SUPPORTS AUTOMATIC DIGITAL SEGMENTATION	No	No	No	Yes	Yes: between regions	No	Yes
ANALYSIS OF REGIONAL VARIABILITY	No	Yes: between regions	No	No	No	No	Yes: between regions, and between sex
FORMAT OF DIGITAL ATLAS	NIfTI	NIfTI	Analyze (AVW 7.5)	NRRD	Not specified	NIfTI	MINC and NIfTI
PURPOSE OF STUDY	Tool for spatial analysis of neuroanatomical location for use in planning and guidance of experimental procedures.	To establish a timeline of morphometric changes and variability throughout neurodevelopment	Stereotaxic MR template with tissue class distribution maps to facilitate use of fMRI software in tissue segmentation of brain data.	Digital atlas based semi-automatic segmentation to increase efficiency of Sprague Dawley analysis at P5, P14, and P72.	Enhance understanding of neuroanatomy of the Wistar rat and offer a collaborative platform for future rat brain studies.	Template set including white and grey matter probabilistic segmentation for use in fMRI localization in Wistar rats.	To develop the first tool for automatic digital segmentation of the Fischer 344 rat brain and to examine regional variability between regions and between sex, allowing more efficient selection of future experiment sample sizes.

Table 1. Comparison between existing atlases and the current study.

As seen in **Table 1**, there are several methods to generate whole brain atlases, as well as several different purposes for such atlases. The current atlas is the first reported atlas of the Fischer 344 rat brain. There are numerous advantages of the present atlas over currently existing rat brain atlases. Firstly, our atlas uses a relatively high number of scans (n=41), as well as using both males and female rats, to produce an average image which reduces bias from any single animal. In comparison, many other atlases only use around 5 subjects and generally only use male animals (Papp et al. 2014; Johnson et al. 2012; Rumple et al. 2013). Using a male-only generated atlas would be problematic when trying to apply the atlas to a mixed sex study because there are clear sexual dimorphisms within regions, as documented thoroughly in the literature (Hines et al. 1992; Shah et al. 2004; Biezonski et al. 2016) as well as demonstrated in the current study. To our knowledge, the rat atlas by Schwarz et al. (2006) is the only one that uses more subjects (n=97 males) than in the current study. However, despite the higher number of rats used to generate their atlas, the image resolution was significantly lower than the present study.

All of the previously published rat atlases provide value to researchers working on different types of projects, whether they are interested in co-registering atlases to stereotaxic coordinates for use in surgery (Papp et al. 2014), to enhance our understanding of early neurodevelopment (Calabrese et al. 2013), or allow semi-automatic segmentation of early-development rat brains (Rumple et al. 2013). That said, the present study reports the highest number of delineated structures (n=98) - except for atlases generated for stereotaxic surgery purposes which use a digitally co-registered P&W atlas - based on a population-averaged template, which was possible due to the high isotropic resolution of the MR template image. Thus, the current study provides novel value by reporting a high-resolution, mixed-sex Fischer 344 rat atlas in MINC and NIfTI format for use in automatic structural segmentation and statistical analysis. Regional variation and structural sexual dimorphisms are also reported.

The practice of creating an MRI-based atlas generally involves generating a template brain using one of two approaches: a group-based approach or a single subject-based approach. The group-based approach takes a group of representative brains and creates an average image using deformation- or voxel- based morphometric algorithms. In contrast, the single subject approach takes a single brain that is deemed to be most representative of the strain and uses that single brain as the template for the atlas. The benefit of the group-based approach is that it produces a high-resolution template while minimizing bias of a single subject, as well as capturing commonalities and variability in the population. Through statistical averaging, the average image can be up-sampled to a higher resolution than the initial subject images. A trade-off of the group-based approach is that small or highly variable regions can be lost due to statistical blurring. In contrast, the single subject approach, especially when used in conjunction with high-resolution ex-vivo imaging, can produce an exceptionally high-resolution MR image, but this is at

the risk of including subject-specific anatomical abnormalities. In this work, we chose to develop an atlas of the Fischer 344 rat strain using a group-based approach. We also chose to use in-vivo MR scans in place of higher resolution ex-vivo scans, as the animals used are also part of an ongoing longitudinal study (unpublished). The described atlas contains 98 delineated structures throughout the whole brain, with an isotropic spatial resolution of 60 µm. The atlas was developed by manual segmentation of a group averaged rat brain and labels were assigned to each individual voxel to identify which voxels correspond to each anatomical structure

The resulting atlas can be utilized in conjunction with standard image processing pipelines used in cross-sectional and longitudinal neuroimaging studies (Biezonski et al, 2016; Chakravarty et al, 2013; Lerch et al, 2017) and to provide structure-specific quantitative volumetric data at the single-subject level (Qiu et al, 2013). By contrasting experimental groups against an appropriate control, this atlas would allow researchers to assess differences in regional brain volumes associated with some experimental or genetic manipulation. Furthermore, longitudinal assessment of volumetric changes is also possible by repeating the co-registration procedure using brain images obtained in the same sample at different timepoints. In practice, the above can be achieved by propagating this atlas onto experimental scans by co-registering individual rat brain scans to the template and using the Multiple Automatically Generated Template brain segmentation algorithm (MAGeT) described in (Chakravarty et al, 2013). Additionally, one of the main strengths of this volumetric atlas is its compatibility with the Pydpiper and RMINC statistical software (Chakravarty et al, 2013; Lerch et al, 2017). The final atlas is provided in both MINC 2.0 (Vincent et al, 2016) and NIfTI (Cox et al, 2004) file formats to maximize utility for the community.

2. METHODS

2.1 Animal:

Forty-four Fischer 344 rats were scanned at four months of age. Due to motion artefacts, 3 MRI scans were excluded from further analysis. The remaining 41 adult Fischer 344 rats (24 males, 17 females) were free of major neuroanatomical abnormalities, based on visual inspection by a trained rater (DG) and were used to create the Fischer 344 atlas. At the time of scanning, the average age of the rats was 112 ± 7 days, and the average weight was 282 ± 60 g. The 41 rats were generated by two separate breeding colonies housed at the Douglas Hospital Research Centre's Animal Facility in Montreal, Canada. Nine rats (3 F, 6 M) were the offspring of hemizygous male TgF344-AD (Tg) rats (acquired through a Material Transfer Agreement with the Terrence Town Laboratory at the University of Southern California) on a Fischer 344 background, bred with F344/NHsd wild-type (WT) females (010; Envigo Laboratories). Offspring from these breeders were a mixture of hemizygous Tg and homozygous

wildtype (WT) rats, produced in approximately a 1:1 ratio per litter, of which only the WT Fischer 344 rats were used for the generation of this atlas. The remaining 32 rats (14 F, 16 M) were the products of F344/NHsd wild-type females bred with F344/NHsd wild-type males (010; Envigo Laboratories). All rats from both breeding schemes were genotyped using real time PCR to ensure none of the offspring for this study had incorporated the two transgenes from the TgF344-AD male breeders (Transnetyx, Cordova, TN). Since the wild-type rats used in this study came from two breeding schemes, an MRI-based structural analysis was conducted which found no significant anatomical differences between the two schemes. Rats of the same sex were group housed (usually two per cage unless they showed signs of aggression), with ad libitum access to food and water. Animals were maintained under standard husbandry conditions on a 12/12 h light cycle, with lights on at 07:00 local time; the room temperature, relative humidity and air exchange were automatically controlled and monitored daily by animal facility staff.

Ethical approval: All applicable international, national, and/or institutional guidelines for the care and use of animals were followed. All animal procedures and experiments were approved by the McGill University Animal Care Committee (UACC).

2.2 MRI Acquisition:

MRI data were acquired at the Douglas Centre d'Imagerie Cérébrale using a 7 Tesla Bruker Biospec 70/30 scanner (Bruker, Billerica MA, USA), with an 86 mm volumetric birdcage coil for transmission and a four-channel surface coil array for signal reception (Bruker). Rats were placed under anesthesia with a mixture of oxygen and isoflurane (4% iso during induction, then 2-4% for maintenance). The isoflurane level was adjusted to maintain a breathing rate between 45-65 breath/min throughout the procedure and warm air (37°C) was blown into the bore of the scanner to maintain a constant body temperature. Animals were kept under anesthesia for 60 minutes while anatomical MRI, fMRI, and MRS data were acquired.

High-resolution 3D anatomical MR images were acquired using Rapid Acquisition with Refocused Echoes (RARE) : TR = 325 ms, echo spacing = 10.8 ms, RARE factor = 6, effective echo time = 32.4 ms, FOV = 20.6 x 17.9 x 29.3 mm, matrix size = 256 x 180 x 157, slice thickness 17.9 mm (along the dorsal/ventral direction), readout along the rostral/caudal direction, scanner resolution = 114 µm isotropic, 19m35s acquisition time. Following the scan, animals were allowed to recover from anesthesia and returned to group housing.

2.3 Image Processing and Registration Pipelines

All images were processed in MINC format. Processing was performed using MINC-toolkit-v2 (https://github.com/BIC-MNI/minc-toolkit-v2) and the Pydpiper module (https://github.com/Mouse-Imaging-Centre/pydpiper; Friedel et al, 2013) was used to co-register the processed images to produce a high-resolution co-registered average isotropic image.

Specimen registration was completed in an iterative process (**Figure 1)** to maximize the quality of the final template brain image using MINC-toolkit and the Pydpiper pipeline. First, raw anatomical MRI data from the scanner were exported in DICOM format and converted into MINC format for image pre-processing. Next, for each image an Otsu-threshold masking procedure was performed (Otsu 1979), followed by an N4 bias field correction (Tustison et al, 2010) in conjunction with the Otsu mask as weighting. The resulting intensity-normalized images were then run through the Pydpiper pipeline MBM.py which performs a co-registration of all input images to produce a group average image. The images initially underwent a rigid 6 parameter (LSQ6) alignment of rotations and translations to situate all images in a common space, followed by an affine 12 parameter (LSQ12) alignment which scales and shears the images pairwise to create an average. Finally, an iterative series of non-linear (nlin) alignments was performed to account for the remaining differences between brains. The output of this pipeline was upsampled to an isotropic resolution of 60 µm and masked to remove surrounding skull and non-brain tissue. Finally, the image was rotated 5 degrees about the z-axis to centre and square the image in the coronal view, resulting in an initial (first stage) group consensus average image.

Using the image labelling tools within the minc-toolkit-v2 program Display, a whole-brain mask was manually generated based on this first stage group average image. Intensity normalizations were re-applied to the raw MRI image files by using the first stage average and whole-brain mask to strictly exclude non-brain regions from re-normalization. The resulting intensity normalized raw images were then run through the Pydpiper MBM.py pipeline using the first stage group average image as an initial model to increase image registration fidelity. The resulting average image with an isotropic resolution of 60 µm was then used as the final template image for the structural segmentation (**Figure 2).**

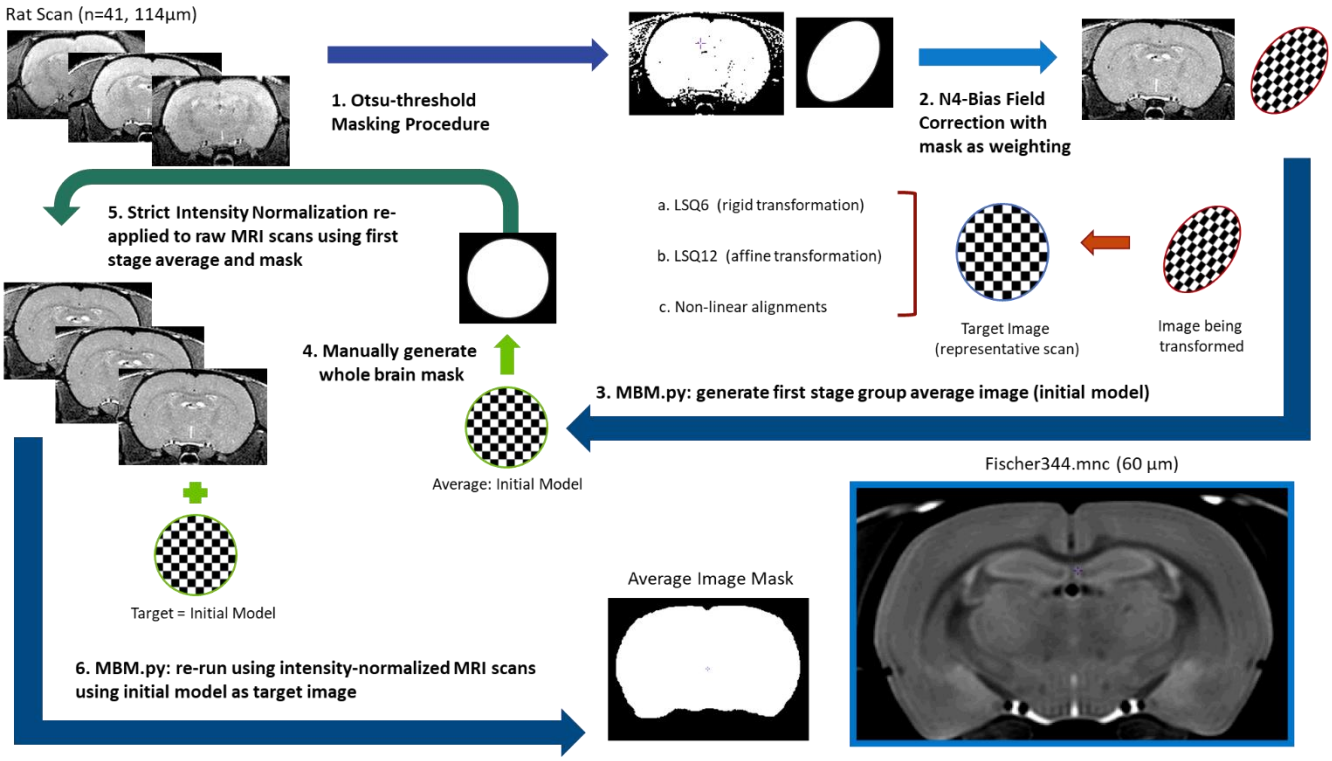

Figure 1: Flow chart demonstrating the iterative process used to produce the template image used for segmentation, as described in Section 2.3.

2.4 Image Segmentation Protocol:

Segmentation was performed by a single investigator (D.G.) based on the combined observations of T_2-weighted tissue contrast as well as the P&W paper atlas (Paxinos and Watson, 2007). Anatomical regions were delineated using the `Display` Software of the MINC-toolkit-v2 version 1.9.16 (https://github.com/BIC-MNI/minc-toolkit-v2). Positive grayscale contrast was used for all manual segmentation tasks. Regions were delineated on each coronal slice individually, and bilaterally, from the olfactory bulb to the first slice of spinal cord. In total, 98 anatomical structures or substructures were manually identified and included in the atlas. In certain specific regions, when boundaries were not obvious on basis of image contrast, the P&W atlas was used to identify the boundary using geometric rules. Such regions are identified in further detail in the delineation section. The majority of the segmentation was done in the coronal view, however both the sagittal and axial views were used to ensure accuracy from other perspectives (**Figure 2**).

First, regions with significant and clear contrast from other regions such as the fibre tracts, ventricles, and caudoputamen were segmented. Next, peripheral brain regions such as the olfactory bulb, brainstem, and cerebellum were delineated. Inner brain nuclei that had poorer regional contrast were then delineated with the use of P&W Rat Brain atlas and by comparison to already delineated surrounding structures. Finally, the neocortex was delineated into 27 major anatomical regions by drawing grid lines

over the template volume and comparing against P&W's delineated neocortex. The regions that were not delineated on the basis of image contrast such as neocortical sub-regions are not intended to prescribe definitive regional volumes and are intended more as a guide of the approximate regional boundaries. As such, these regions are collapsed into the larger definition of *neocortex* in the quantitative analyses reported in **Table 2** and **Table 3.** A complete description of the methodology used to delineate individual structures can be found in the **Supplementary Methods Section**.

The resulting atlas MINC file contains numbered labels that correspond to each substructure, and a hierarchical Excel (.xlsx) file (https://www.nearlab.xyz/fischer344atlas) contains information about the label number and the region of the brain that the label represents. This allows RMINC statistical software, for example, in a longitudinal deformation-based analysis, to identify regions of atrophy or growth by mapping the labeled atlas to the subject at various time points.

The use of atlas labeling, in conjunction with the label hierarchy file provided will allow researchers to tailor the level of regional specificity desired for a given study. For example, the neocortical regions could be analysed at the level of individual cortical regions such as Somatosensory Area 1 (S1) and Motor Area 1 (M1), at the level of cortical lobes such as Frontal Lobe and Parietal Lobe, or at the level of the complete neocortex itself. This hierarchical labeling feature allows the Fischer 344 atlas to be optimized to the detail of analysis that the study requires.

2.5 Statistical Analysis:

The RMINC package in the R statistical environment was used to calculate the average volumes for each structure across all subjects (n=41) and to perform statistical comparisons between male (n=24) and female (n=17) volumes. The atlas label file was mapped to individual scans used in the analysis via the RMINC function `anatGetAll` which resulted in each voxel in each individual scan being uniquely labelled with a structural label. When mapping each rat brain to a common space, a MINC file containing the Jacobian determinant of each voxel required to scale the scan to the common space is generated. The RMINC function `anatGetAll` computes the structural volume for each region in mm^3 by multiplying this scaling factor at each voxel by the voxel size and summing each value within each unique label. For the whole cohort average volume, the volume for each structure was averaged across the cohort, and standard deviation was computed.

For the sex-differences analysis, a two-sample, two-tailed Student's T-test was performed with a Benjamini-Hochberg FDR correction (q=0.05) to control for multiple comparisons. The relative volume of each structure normalized to the volume of the subject's total brain volume was computed to assay relative differences between male and female brain regions, reported in **Table 3**. In addition, the

mean and standard deviations of regional volumes across the whole sample as well as for male and female rats are reported in **Table 2**.

2.6 Data Sharing:

The final anatomical segmentation volume along with the template brain, corresponding label descriptions, and a brain masking volume were each converted from MINC format into NIfTI format using the minc-toolkit `mnc2nii` function. All of the above are available for download and free use through the Near Lab website at https://www.nearlab.xyz/fischer344atlas in both NIfTI and the MINC 2.0 format – compatible with all MINC tools, as well as Pydpiper and RMINC software.

3. RESULTS

In this Fischer 344 rat atlas, we delineated 98 anatomical structures including the ventricular system, grey matter, and white matter tracts. The level of detail in the averaged brain template is exemplified along with an overview of the anatomical delineations in **Figures 2** and **3**. It should be noted that good image contrast in the template has allowed for relatively detailed delineations in the cerebellum (**Figure. 4**). Based on the anatomical labels, and using the methods described in **Section 2.5**, regional volumes for regions distinguishable based on T2-weighted contrast were calculated for each of the 41 brains. Average volumes for each region, as well as the level of variability within and across male and female animals are summarized in **Table 2**.

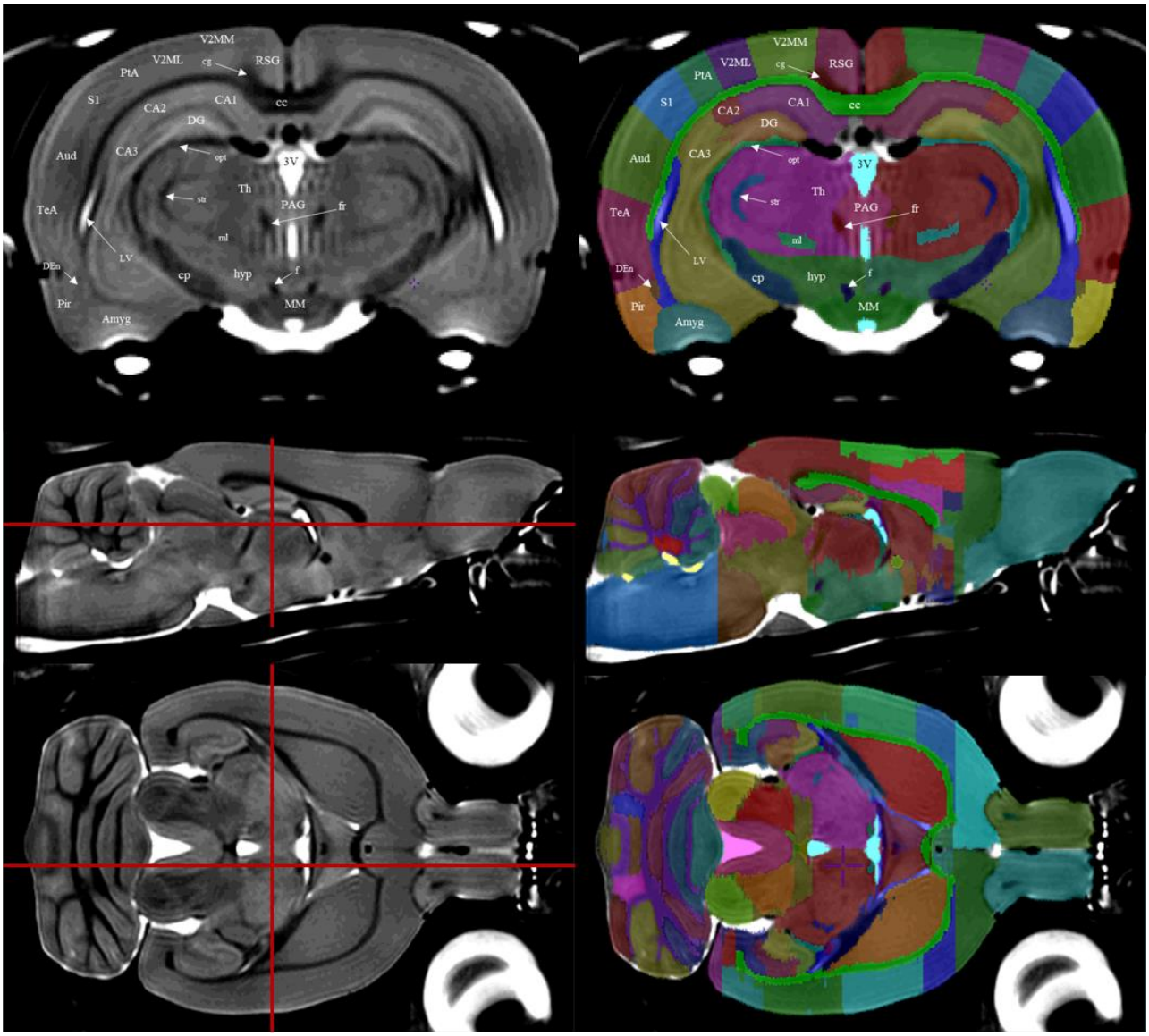

Figure 2: Left column: the averaged brain, which served as a template for structural delineation. Red crosshairs on transverse and sagittal view (middle and bottom) indicate the positions of the other planes. **Right column:** the atlas file is overlaid onto the template file. Delineation and refinement were primarily performed using the coronal sections, though further refinement was done in both the sagittal and axial planes. **Top row:** annotated over the left hemisphere of both coronal images are the structural regions that the label tags represent. **Middle** and **Bottom row** show transverse and sagittal views respectively. Aud, auditory cortex; Amyg, amygdala;CA1, CA1 field of the Hippocampus; CA2, CA2 field of the hippocampus; CA3, CA3 field of the hippocampus; CC, corpus callosum and associated white matter; cg, cingulum; cp, cerebral peduncles; DG, dentate gyrus; DEn, dorsal endopiriform nucleus; f, fornix; fr, fasciculus retroflexus; hyp, hypothalamus; LV, lateral ventricle; ml, medial lemniscus; MM, mammillary bodies; opt, optic tract; PAG, periaqueductal gray; Pir, piriform cortex; PtA, parietal association cortex; RSG, retrosplenial granular cortex; S1; primary somatosensory cortex; TeA, temporal association cortex; V2ML, secondary visual cortex, lateral area; V2MM, secondary visual cortex, medial area; 3V, third ventricle.

VENTRICULAR SYSTEM	ALL SUBJECTS MEAN + SD (mm^3)	MALES MEAN + SD (mm^3)	FEMALES MEAN + SD (mm^3)
Aqueduct	2.11 ± 0.27	2.3 ± 0.23	1.92 ± 0.16
Fourth ventricle	3.07 ± 0.43	3.37 ± 0.29	2.76 ± 0.11
Lateral ventricle	13.24 ± 0.83	13.82 ± 0.56	12.65 ± 0.31
Third Ventricle	5.13 ± 0.31	5.35 ± 0.15	4.92 ± 0.17

GREY MATTER STRUCTURE	ALL SUBJECTS MEAN + SD (mm^3)	MALES MEAN + SD (mm^3)	FEMALES MEAN + SD (mm^3)
Basal Forebrain	23.43 ± 1.62	24.57 ± 0.84	22.29 ± 0.4
Bed Nucleus of the Stria Terminalis	3.47 ± 0.33	3.7 ± 0.1	3.24 ± 0.08
Caudoputamen	73.67 ± 3.63	76.24 ± 2.09	71.1 ± 1.71
Cerebellar Lobule 1 & 2	13.47 ± 1.25	14.35 ± 0.48	12.59 ± 0.41
Cerebellar Lobule 10	3.29 ± 0.26	3.47 ± 0.16	3.1 ± 0.12
Cerebellar Lobule 3	12.7 ± 0.81	13.28 ± 0.52	12.13 ± 0.34
Cerebellar Lobule 4 & 5	32.84 ± 2.25	34.43 ± 1.33	31.25 ± 0.79
Cerebellar Lobule 6	11.78 ± 1.04	12.52 ± 0.63	11.05 ± 0.48
Cerebellar Lobule 7	4.46 ± 0.3	4.68 ± 0.21	4.25 ± 0.17
Cerebellar Lobule 8	4.84 ± 0.37	5.1 ± 0.29	4.58 ± 0.22
Cerebellar Lobule 9	10.54 ± 0.96	11.22 ± 0.41	9.86 ± 0.25
Cochlear Nucleus	1.89 ± 0.15	2 ± 0.06	1.79 ± 0.04
Copula	3.59 ± 0.37	3.86 ± 0.12	3.33 ± 0.08
Crus 1 Ansiform Lobule	24.43 ± 1.66	25.61 ± 0.99	23.26 ± 0.59
Crus 2 Ansiform Lobule	10.61 ± 0.71	11.12 ± 0.54	10.11 ± 0.29

Dentate Gyrus	22.9 ± 1.95	24.28 ± 0.9	21.52 ± 0.61
Dentate Nucleus	1.99 ± 0.15	2.1 ± 0.08	1.88 ± 0.03
Fastigial Nucleus	2.33 ± 0.17	2.45 ± 0.08	2.21 ± 0.06
Flocculus	10.67 ± 0.78	11.22 ± 0.52	10.12 ± 0.56
Globus Pallidus	7.85 ± 0.42	8.15 ± 0.28	7.55 ± 0.23
Hindbrain	164.08 ± 13.17	173.39 ± 5.91	154.77 ± 3.57
Hippocampal CA1 field	36.36 ± 2.65	38.23 ± 1.13	34.49 ± 1.17
Hippocampal CA2 field	3.63 ± 0.23	3.8 ± 0.14	3.47 ± 0.18
Hippocampal CA3 field	27.12 ± 1.73	28.34 ± 0.85	25.89 ± 1.04
Hypothalamus	41.83 ± 2.98	43.94 ± 1.41	39.72 ± 0.67
Inferior Colliculus	25.24 ± 1.31	26.16 ± 0.9	24.31 ± 0.61
Interposed Nucleus	2.58 ± 0.17	2.7 ± 0.08	2.46 ± 0.05
Lateral Septum	12.98 ± 0.77	13.52 ± 0.41	12.43 ± 0.28
Mammillary Bodies	2.09 ± 0.13	2.18 ± 0.09	2 ± 0.07
Medial Septum	2.07 ± 0.12	2.15 ± 0.08	1.98 ± 0.06
Median Preoptic Area	0.08 ± 0.003	0.08 ± 0.003	0.08 ± 0.0028
Midbrain	64.2 ± 5.1	67.81 ± 2.42	60.59 ± 0.97
Neocortex	630.9 ± 39.3	653.25 ± 24.3	599.34 ± 22.6
Nucleus Accumbens	13.58 ± 0.6	14.01 ± 0.43	13.15 ± 0.35
Olfactory Bulb	129.89 ± 10.32	137.19 ± 4.9	122.6 ± 2.97
Paraflocculus	14.06 ± 1.06	14.81 ± 0.63	13.31 ± 0.63
Paramedian Lobule	10.87 ± 0.86	11.48 ± 0.44	10.26 ± 0.21
Periaqueductal Grey	15.18 ± 0.75	15.71 ± 0.4	14.65 ± 0.28
Pons	44.99 ± 3.29	47.32 ± 2.13	42.66 ± 0.98

Simple Lobule	22.8 ± 1.49	23.86 ± 0.69	21.75 ± 0.72
Subfornical Organ	0.13 ± 0.01	0.14 ± 0.01	0.12 ± 0.01
Substantia Nigra	4.68 ± 0.33	4.91 ± 0.23	4.45 ± 0.09
Superior Colliculus	27.11 ± 1.81	28.39 ± 0.96	25.83 ± 0.77
Thalamus	73.61 ± 4.12	76.52 ± 2.22	70.7 ± 1.84
Ventral Pallidum	4.06 ± 0.24	4.23 ± 0.12	3.89 ± 0.08

WHITE MATTER STRUCTURE	**ALL SUBJECTS MEAN + SD (mm^3)**	**MALES MEAN + SD (mm^3)**	**FEMALES MEAN + SD (mm^3)**
Anterior Commissure, anterior part	2.67 ± 0.16	2.78 ± 0.09	2.55 ± 0.07
Anterior Commissure, intra-bulbar part	0.64 ± 0.05	0.68 ± 0.02	0.61 ± 0.02
Anterior Commissure, posterior part	1.66 ± 0.09	1.72 ± 0.06	1.6 ± 0.05
Cerebral Peduncle	6.24 ± 0.38	6.51 ± 0.27	5.97 ± 0.13
Cingulum	7.06 ± 0.52	7.43 ± 0.27	6.69 ± 0.2
Commissure of the Inferior Colliculus	0.63 ± 0.01	0.64 ± 0.02	0.62 ± 0.02
Commissure of the Superior Colliculus	0.32 ± 0.03	0.34 ± 0.02	0.3 ± 0.01
Corpus Callosum and Associated White Matter	63.9 ± 4.25	66.9 ± 2.19	60.89 ± 2.08
External Medullary Lamina	1.32 ± 0.1	1.39 ± 0.05	1.25 ± 0.03
Fasciculus Retroflexus	0.36 ± 0.02	0.37 ± 0.01	0.34 ± 0.01
Fimbria	7.21 ± 0.56	7.6 ± 0.25	6.82 ± 0.25
Fornix	0.88 ± 0.06	0.92 ± 0.03	0.84 ± 0.02

Internal Capsule	15.38 ± 0.99	16.08 ± 0.61	14.68 ± 0.41
Lateral Olfactory Tract	2.5 ± 0.18	2.63 ± 0.1	2.38 ± 0.06
Mammillothalamic Tract	0.46 ± 0.02	0.47 ± 0.01	0.44 ± 0.01
Optic Chiasm	0.52 ± 0.08	0.58 ± 0.04	0.46 ± 0.03
Optic Tract	6.34 ± 0.58	6.75 ± 0.24	5.93 ± 0.17
Posterior Commissure	0.29 ± 0.02	0.3 ± 0.02	0.27 ± 0.01
Stria Medullaris of the Thalamus	1.06 ± 0.07	1.1 ± 0.03	1.01 ± 0.03
Stria Terminalis	3.2 ± 0.23	3.36 ± 0.14	3.04 ± 0.1
Trochlear Nerve	0.21 ± 0.01	0.22 ± 0.01	0.21 ± 0.01
Cerebellar White Matter/ Arbor Vitae	47.14 ± 3.48	49.6 ± 1.52	44.68 ± 0.97

Table 2. Regional volumes calculated for each label region as described in **Section 2.5 Statistical Analysis**, and averaged across brains. 71 delineated structures along with their corresponding mean and standard deviation (mm^3) across all subjects (n=41), male rats (n=24) and female rats (n=17) are reported as the neocortical regions were collapsed into a single region of analysis— called neocortex.

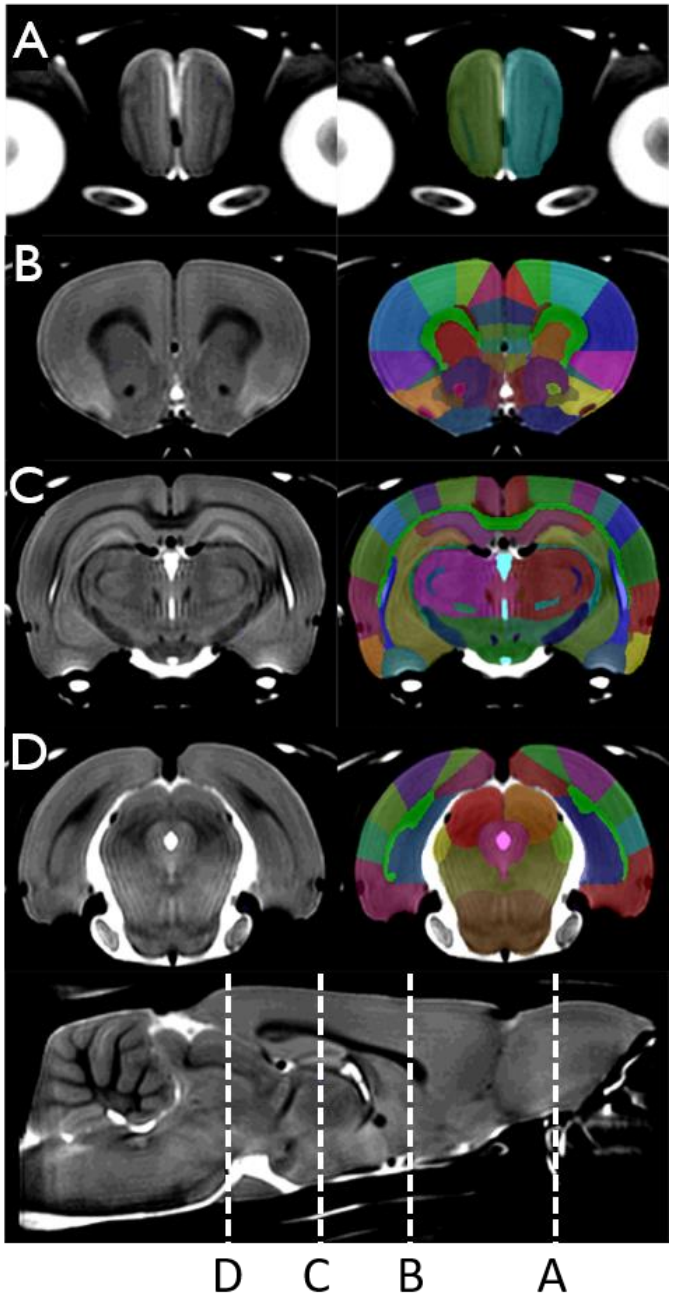

Figure 3: In the **left column** is the template brain, and in the **right column** is the template brain with the atlas file superimposed. This figure shows a series of coronal slices at different regions of the neocortex. The positions of representative slices are marked with dashed lines in a mid-sagittal slice with labels A-D.

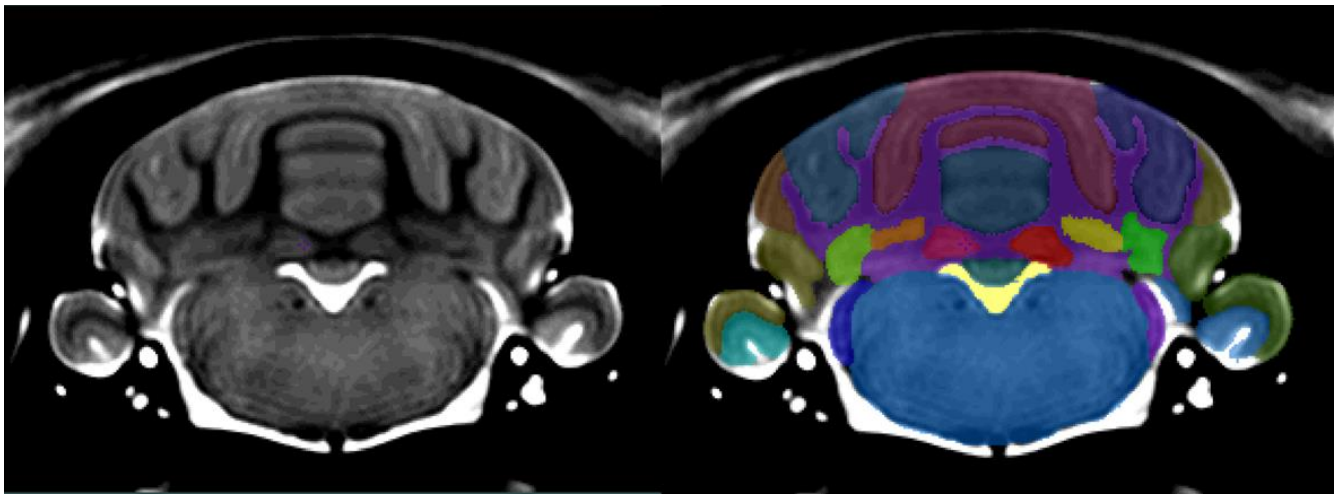

Figure 4: On the **left** is the template brain, and on the **right** is the template brain with the atlas file superimposed. Clear boundaries are identifiable between all of the major lobes. White matter and Arbor Vitae were indistinguishable from each other based on the resolution of the image. All the hindbrain nuclei were delineated as one structure due to poor resolution and low contrast levels in the hindbrain.

In addition to delineation of 98 anatomical structures in this Fischer 344 atlas, we report an analysis of the variability of regional brain volumes across 41 Fischer 344 rats, as well as a novel analysis of sex differences in regional brain volumes. This data may assist researchers to better plan sample sizes when designing experiments aimed at detecting significant treatment effects from random variation in Fischer 344 rats (Lerch et al, 2012). On average, the variability of brain regions across all samples expressed in terms of percent of the region volume was 5% (**Figure 5**), indicating that there are fairly small regional variations across four-month-old Fischer 344 rats. In the ventricular system the variability reached 14.2% (4^{th} ventricle), which can possibly be attributed to differences in hydration levels between subjects resulting in variant CSF levels.

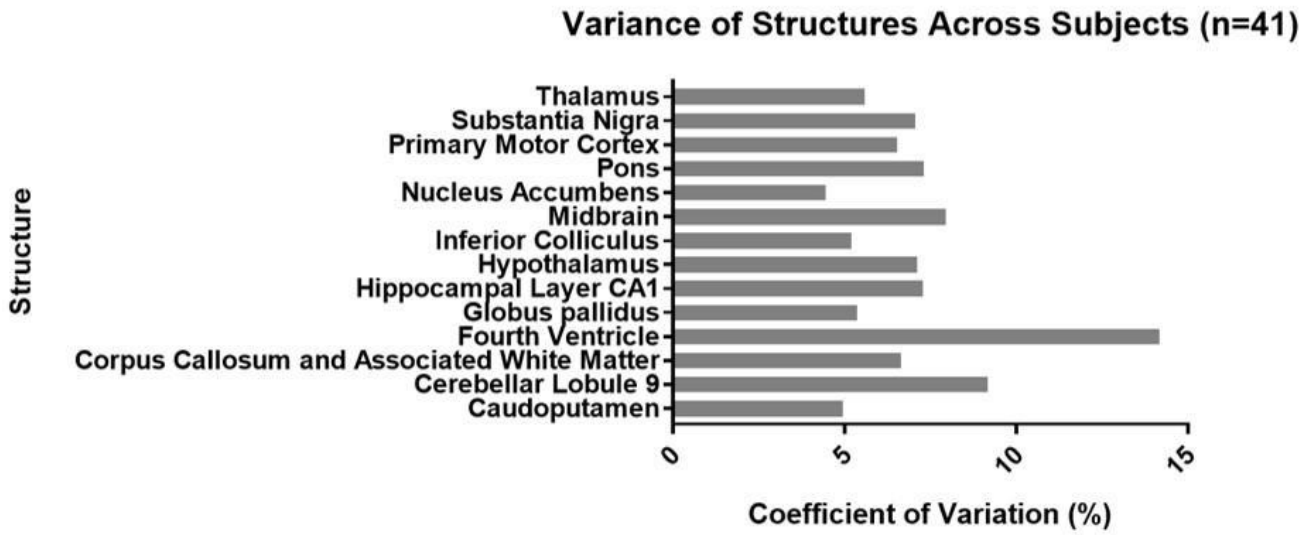

Figure 5: Comparison of the coefficient of variation (CV) for selected structures across all 41 subjects. The volume of most of the 98 structures varies between 5% and 8% across subjects. As expected, the ventricular system displays increased variation across subjects (14.2%).

We performed two different analyses to compare structural volumes (Qiu et al, 2013) between male and female rats. First, we assessed the absolute volumes of each region to evaluate which regions were significantly different in size. Next, we looked at relative volumes (absolute regional volume divided by whole brain volume) to evaluate differences between the relative regional volumes between sexes. When evaluating absolute size differences between sexes, all regions were significantly larger in males relative to females (see **Supplemental Table 1** for more details). This is understandable due to animal size differences—the mean total volume of the male brains was 2002 ± 64 mm^3 while the mean total volume of female brains was 1819 ± 37 mm^3. In contrast, when evaluating relative volumes, certain volumes were significantly larger in females. **Table 3** reports the results of a two-tailed t-test with correction for multiple comparisons between the relative regional volumes between male and female Fischer 344 rats. One specific finding of interest is that females have a relatively larger neocortex ($p<0.001$). Many of the other regions that were also found to be significantly larger in females were fibre tracts involved in cortico-cortical communication such as the internal capsule, anterior commissure and the commissures of the colliculi. These findings are logical: since the neocortex is relatively larger, the fibre tracts that connect the different cortical regions would also be expected to be larger.

STRUCTURE	P-VALUE	DIRECTION OF GREATER RELATIVE VOLUME
Anterior Commissure, anterior part	3.53E-01	Female

Anterior Commissure, intra-bulbar part	1.49E-04	Female
Anterior Commissure, posterior part	2.28E-04	Female
Cerebral Peduncle	2.95E-03	Female
Cingulum	7.00E-01	Female
Commissure Inferior Colliculus	3.70E-07	Female
Commissure Superior Colliculus	3.89E-01	Male
Corpus Callosum and Associated White Matter	4.21E-02	Female
External Medullary Lamina	7.64E-01	Male
Fasciculus Retroflexus	6.13E-03	Female
Fimbria	6.70E-01	Male
Fornix	9.32E-04	Female
Internal Capsule	1.47E-03	Female
Lateral Olfactory Tract	1.64E-01	Female
Mammillothalamic Tract	4.35E-06	Female
Optic Chiasm	2.26E-06	Male
Optic Tract	5.37E-04	Male
Posterior Commissure	9.84E-01	Male
Stria Medullaris Thalamus	3.71E-02	Female
Stria Terminalis	3.78E-01	Female
Trochlear Nerve	6.25E-06	Female
White Matter of Cerebellum	6.06E-01	Female
Basal Forebrain	2.81E-02	Female
Bed Nucleus of the Stria Terminalis	1.33E-05	Male
Caudoputamen	1.52E-13	Female

Cerebellar molecular layer 1 & 2	4.53E-03	Male
Cerebellar molecular layer 10	5.89E-01	Male
Cerebellar molecular layer 3	5.32E-02	Female
Cerebellar molecular layer 4 & 5	1.52E-01	Female
Cerebellar molecular layer 6	1.16E-01	Male
Cerebellar molecular layer 7	3.13E-01	Female
Cerebellar molecular layer 8	9.05E-01	Male
Cerebellar molecular layer 9	5.47E-04	Male
Cochlear Nucleus	3.85E-01	Male
Copula	1.64E-07	Male
Crus 1 Ansiform Lobe	1.19E-01	Female
Crus 2 Ansiform Lobe	2.28E-01	Female
Dentate Gyrus	4.45E-03	Male
Dentate Nucleus	9.31E-01	Male
Fastigial Nucleus	6.40E-01	Female
Flocculus	7.32E-01	Female
Globus Pallidus	6.90E-05	Female
Hindbrain	1.69E-01	Male
Hippocampal CA1 field	4.97E-01	Female
Hippocampal CA2 field	1.52E-01	Female
Hippocampal CA3 field	2.80E-02	Female
Hypothalamus	1.48E-01	Female
Inferior Colliculus	1.41E-05	Female
Interposed Nucleus	1.00E-01	Female
Lateral Septal Complex	5.61E-05	Female

Mamillary Bodies	3.30E-02	Female
Medial Septal Complex	2.44E-03	Female
Median Preoptic Area	2.20E-05	Female
Midbrain	1.32E-01	Male
Neocortex	5.40E-08	Female
Nucleus Accumbens Core and Shell	7.22E-09	Female
Olfactory Bulb	2.98E-01	Male
Paraflocculus	9.88E-01	Female
Paramedian Lobe	4.29E-01	Male
Periaqueductal Grey	2.45E-07	Female
Pons	5.97E-01	Female
Simple Lobule	6.41E-02	Female
Subfornical Organ	2.50E-02	Male
Substantia Nigra	3.73E-01	Female
Superior Colliculus	4.11E-02	Female
Thalamus	6.48E-09	Female
Ventral Pallidum	1.61E-04	Female
Aqueduct	1.57E-02	Male
Fourth ventricle	7.68E-05	Male
Lateral ventricle	1.50E-02	Female
Third Ventricle	2.64E-02	Female

1.94

Table 3. Two sample, two tailed t-test between the relative volumes of Male (n=24) and Female (n=17) groups. The second column indicates the p-value obtained from the t-test. Regions with significant relative volume differences between males and females after FDR correction are highlighted in green. The third column indicates the direction of greater relative volume. Of specific interest is the neocortex with females having significantly ($p<0.0001$) larger relative neocortex than males. In this

analysis, all 27 neocortex segmentations were collapsed into one structure (neocortex) in order to view the macroscopic differences between male and female cortices.

4. DISCUSSION

In the present study we developed a 60 μm isotropic template image of the normative Fischer 344 rat brain, from which we created an atlas comprised of 98 structures and provided a detailed basis for delineation for each structure. We present these tools along with a template brain masking file in both the MINC 2.0 and NIfTI imaging file format as open-access tools available to researchers to validate as well as to facilitate highly detailed structural analyses.

This paper presents a tool for preclinical researchers to identify brain structures within MR images of the Fischer 344 rat brain in a digital format, enabling semi-automated structural analyses to be performed and thus expediting the process of data analysis. Additionally, due to the automated nature of the identification of brain regions using software such as MAGeT or RMINC, segmentation bias is reduced across subjects. As rat brain development is completed by the end of adolescence, or post-natal day 45, this tool can be reliably used on most adult Fischer 344 MR images. In order to minimize segmentation inaccuracies, when mapping a set of Fischer 344 volumes to our template image, volumes should be within 10% of the template image volume: 1912 mm^3 (Rumple et al, 2013).

Though other atlases such as the gold standard Paxinos and Watson histological atlas may be able to provide more precise identification of smaller nuclei that is not attainable on an in-vivo MRI based atlas presented in this paper, this Fischer 344 rat brain atlas provides the rodent neuroimaging community with the first Fischer 344 rat brain MRI atlas, a high resolution template isotropic image and label hierarchy that can be tailored to the desired anatomical specificity of analysis (i.e. S1 or Frontal Lobe).

Furthermore, the absolute volumes of each anatomical region across the whole group, as well as between sexes reported in **Table 2** provide valuable information to researchers attempting to plan future studies. This data will allow researchers to better plan sample sizes when performing a longitudinal study of regional atrophy, for example. Highly detailed data on the structural volumes of Fischer 344 rat brains is not documented in the literature, and thus this analysis provides novel value for future investigations.

This resource was developed using scans taken from 41 four-month old male and female Fischer 344 wild-type rats weighing 282g ± 60g. 32 of the subjects were wild-type (WT/WT) offspring from homozygous wild-type breeders, and 9 were wild-type (WT/WT) offspring from a hemizygous (WT/Tg) transgenic male bred with a homozygous wild-type female (WT/WT). A structural comparison using the Pydpiper pipeline confirmed that there is no structural variance between the wild-type rats that came from different lineages.

The present work has some limitations, outlined below:

- The raw scan resolution of 114 µm may not allow delineation of very small structures. Additionally, adjacent grey matter nuclei, such as the thalamic nuclei, are very difficult to distinguish, and therefore are not delineated in this atlas.
- Some regional boundaries such as the neocortical boundaries are not discernable based on tissue contrast. In order to consistently delineate these structures, we used gridlines in conjunction with the Paxinos and Watson paper atlas, but this method is not without potential biases.
- All rats used for this study were four months of age and are therefore considered to have reached mature adulthood. However, due to normal changes in brain shape and volume during the rat lifespan, this atlas may not be applicable to significantly older or younger rats.
- The sample sizes between male and female rats were uneven, with 24 male rats and 17 female rats. This could have the effect of over-weighting the structural differences that are observed in the male rats.
- Even though all of the rats used in this study were homozygous WT, they came from two different backgrounds: 32 from homozygous WT/WT breeders and 9 from hemizygous WT/Tg (TgF344-AD) breeders. However, any effects of parental background are likely minimal, since a separate structural analysis found no significant anatomical differences between the homozygous wildtype rats bred from WT/WT and WT/Tg parental backgrounds used in this study.
- Manual segmentation of all structures was performed in the coronal plane. Even though the transverse and sagittal views were inspected to ensure spatial continuity of the various anatomical structures, it is impossible to guarantee smoothness of the structural boundaries in all three dimensions.

Ever increasing amounts of data are being generated in pre-clinical studies of rodent models, primarily due to the development of better techniques to generate MR images (Barkhof, 2012). The Fischer 344 brain atlas presented in this paper can be used in pre-clinical trials to quickly and precisely identify anatomical regions and their volumes. The advantages of this tool are three-fold. First, this digital atlas allows researchers to expediently process large datasets by semi-automating the process of anatomical analysis and eliminating manual paper-based anatomical analysis. Second, this atlas reduces subject-wise bias in segmentation as all experimental subjects are mapped to the same set of labels. Third, this digital atlas can be used in combination with statistical software such as RMINC in the R environment to perform group-wise regions-of-interest comparisons. Our aim was to provide a novel tool for researchers working with Fischer 344 rats and thus we provide all files for open download at at https://www.nearlab.xyz/fischer344atlas.

References

Balogová, Z., Popelář, J., Chiumenti, F., Chumak, T., Burianová, J. S., Rybalko, N., & Syka, J. (2018). Age-Related Differences in Hearing Function and Cochlear Morphology between Male and Female Fischer 344 Rats. Frontiers in aging neuroscience, 9, 428. doi:10.3389/fnagi.2017.00428

Biezonski, D., Shah, R., Krivko, A., Cha, J., Guilfoyle, D. N., Hrabe, J., . . . Posner, J. (2016). Longitudinal magnetic resonance imaging reveals striatal hypertrophy in a rat model of long-term stimulant treatment. Translational Psychiatry, 6(9). doi:10.1038/tp.2016.158

Calabrese, E., Badea, A., Watson, C., & Johnson, G. A. (2013). A quantitative magnetic resonance histology atlas of postnatal rat brain development with regional estimates of growth and variability. Neuroimage, 71, 196-206.

Chakravarty, M. M., Steadman, P., van Eede, M. C., Calcott, R. D., Gu, V., Shaw, P., ... & Lerch, J. P. (2013). Performing label-fusion-based segmentation using multiple automatically generated templates. Human brain mapping, 34(10), 2635-2654.

Chen, X. J., Kovacevic, N., Lobaugh, N. J., Sled, J. G., Henkelman, R. M., & Henderson, J. T. (2006).Neuroanatomical differences between mouse strains as shown by high-resolution 3D MRI. NeuroImage, 29(1), 99-105. doi:10.1016/j.neuroimage.2005.07.008

Cohen, R. M., Rezai-Zadeh, K., Weitz, T. M., Rentsendorj, A., Gate, D., Spivak, I., et al. (2013). A Transgenic Alzheimer Rat with Plaques, Tau Pathology, Behavioral Impairment, Oligomeric Abeta, and Frank Neuronal Loss. J. Neurosci. 33, 6245–6256. doi: 10.1523/JNEUROSCI.3672-12.2013

Cox, R.W. & Ashburner, John & Breman, H & Fissell, Kate & Haselgrove, C & Holmes, C.J. & Lancaster, J.L. & Rex, D.E. & Smith, S.M. & Woodward, J.B. & Strother, Stephen. (2004). A (sort of) new image data format standard: NiFTI-1. 10th Annual Meeting of the Organization for Human Brain Mapping. 22.

Dorr, A. E., Lerch, J. P., Spring, S., Kabani, N., & Henkelman, R. M. (2008). High resolution three-dimensional brain atlas using an average magnetic resonance image of 40 adult C57Bl/6J mice. Neuroimage, 42(1), 60-69.

Fole, A., Miguéns, M., Morales, L.C., González-Martín, C., & Olmo, N.D. (2017). Lewis and Fischer 344 rats as a model for genetic differences in spatial learning and memory: Cocaine effects. Progress in Neuro-Psychopharmacology and Biological Psychiatry, 76, 49-57.

Friedel, M., van Eede, M. C., Pipitone, J., Chakravarty, M. M., & Lerch, J. P. (2014). Pydpiper: a flexible toolkit for constructing novel registration pipelines. Frontiers in Neuroinformatics, 8, 67. http://doi.org/10.3389/fninf.2014.00067

Hines, M., Allen, L. S., & Gorski, R. A. (1992). Sex differences in subregions of the medial nucleus of the amygdala and the bed nucleus of the stria terminalis of the rat. Brain Research, 579(2), 321-326. doi:10.1016/0006-8993(92)90068-k

Johnson, G. A., Calabrese, E., Badea, A., Paxinos, G., & Watson, C. (2012). A multidimensional magnetic resonance histology atlas of the Wistar rat brain. Neuroimage, 62(3), 1848-1856.

Lancelot S, Roche R, Slimen A, Bouillot C, Levigoureux E, et al. (2014) A Multi-Atlas Based Method for Automated Anatomical Rat Brain MRI Segmentation and Extraction of PET Activity. PLOS ONE 9(10): e109113. https://doi.org/10.1371/journal.pone.0109113

Lerch J, Hammill C, van Eede M, Cassel D (2017). RMINC: Statistical Tools for Medical Imaging NetCDF (MINC) Files. R package version 1.5.2.1

Nowinski, W. L. (2016). Usefulness of brain atlases in neuroradiology: Current status and future potential. The Neuroradiology Journal, 29(4), 260–268. https://doi.org/10.1177/1971400916648338

Otsu, Nobuyuki. (1979). A Threshold Selection Method from Gray-Level Histograms. Systems, Man and Cybernetics, IEEE Transactions on. 9. 62-66

Papp EA, Leergaard TB, Calabrese E, Johnson GA, Bjaalie JG (2014) "Waxholm Space atlas of the Sprague Dawley rat brain" NeuroImage 97:374-386. [doi 10.1016/j.neuroimage.2014.04.001]

Paxinos, George; Watson, Charles. (2007). The Rat Brain in Stereotaxic Coordinates. London: Academic Press.

Perkins, A. E., Piazza, M. K., & Deak, T. (2018). Stereological Analysis of Microglia in Aged Male and Female Fischer 344 Rats in Socially Relevant Brain Regions. Neuroscience, 377, 40-52. doi:10.1016/j.neuroscience.2018.02.028

Qiu, L. R., Germann, J., Spring, S., Alm, C., Vousden, D. A., Palmert, M. R., & Lerch, J. P. (2013). Hippocampal volumes differ across the mouse estrous cycle, can change within 24hours, and associate with cognitive strategies. NeuroImage, 83, 593-598. doi:10.1016/j.neuroimage.2013.06.074

Rumple A, McMurray M, Johns J, Lauder J, Makam P, et al. (2013) 3-Dimensional Diffusion Tensor Imaging (DTI) Atlas of the Rat Brain. PLOS ONE 8(7): e67334.https://doi.org/10.1371/journal.pone.0067334

Schwarz, A. J., Danckaert, A., Reese, T., Gozzi, A., Paxinos, G., Watson, C., ... & Bifone, A. (2006). A stereotaxic MRI template set for the rat brain with tissue class distribution maps and co-registered anatomical atlas: application to pharmacological MRI. Neuroimage, 32(2), 538-550.

Shah, N. M., Pisapia, D. J., Maniatis, S., Mendelsohn, M. M., Nemes, A., & Axel, R. (2004). Visualizing Sexual Dimorphism in the Brain. Neuron, 43(3), 313-319. doi:10.1016/j.neuron.2004.07.008

Tustison, N. J., Avants, B. B., Cook, P. A., Zheng, Y., Egan, A., Yushkevich, P. A., & Gee, J. C. (2010). N4ITK: Improved N3 Bias Correction. IEEE Transactions on Medical Imaging, 29(6), 1310–1320. http://doi.org/10.1109/TMI.2010.2046908

Valdés-Hernández PA, Sumiyoshi A, Nonaka H, Haga R, Aubert-Vásquez E, Ogawa T, Iturria-Medina Y, Riera JJ, Kawashima R (2011) "An in vivo MRI template set for morphometry, tissue segmentation, and fMRI localization in rats" Front Neuroinform 5(26). [doi 10.3389/fninf.2011.00026]

Vincent, R. D., Neelin, P., Khalili-Mahani, N., Janke, A. L., Fonov, V. S., Robbins, S. M., Baghdadi, L., Lerch, J., Sled, J. G., Adalat, R., MacDonald, D., Zijdenbos, A. P., Collins, D. L., … Evans, A. C. (2016). MINC 2.0: A Flexible Format for Multi-Modal Images. Frontiers in neuroinformatics, 10, 35. doi:10.3389/fninf.2016.00035